Magnetic Euripi in Corannulene

Guglielmo Monaco,[†] Lawrence T. Scott,[‡] and Riccardo Zanasi*,[†]

Dipartimento di Chimica, Università degli Studi di Salerno, via Ponte don Melillo, 84084 Fisciano (SA), Italy, and Merkert Chemistry Center, Boston College, Chestnut Hill, Massachusetts 02467-3860

Received: May 2, 2008; Revised Manuscript Received: June 17, 2008

Ab initio current densities induced by an external magnetic field have been computed for corannulene dianion, dication, and tetraanion. The π-ring currents are found to be large with respect to benzene and to undergo remarkable changes in response to variations in the oxidation state. According to the results obtained here, the three corannulene ions plus the neutral species constitute a very special set that spans all of the possible patterns of rim and hub circulations: diatropic/hub-paratropic/rim (the dianion), paratropic/hub-paratropic/rim (the dication, assuming conformationally averaged current density), diatropic/hub-diatropic/rim (the tetraanion), and paratropic/hub-diatropic/rim (the neutral, as already reported by other authors). Orbital contributions and their breakdown into explicit contributions from virtual excitations have been analyzed. It is shown that the dianion and dication are both (2p) systems characterized by a single highest occupied molecular orbital (HOMO)−lowest unoccupied molecular orbital (LUMO) rotationally allowed transition. For the dianion, this transition is responsible not only for the outer paratropic circulation but also for the inner diatropic circulation, a behavior that requires an extension of the few electron model based on orbital contributions to be fully rationalized. For the dication, the HOMO−LUMO transition provides a paratropic circulation localized on one indene subunit. However, because of the fast exchange of conformers, it is sensible to calculate an averaged current density field, which is characterized by con-rotating paratropic inner and outer ring currents. For the tetraanion, the calculated current pattern is in agreement with a previous indication, while the orbital analysis reveals that the HOMO and the HOMO − 1 contribute to both inner and outer circulations. Despite the small 6-31G** basis set employed to calculate current densities and magnetic properties, a satisfactory agreement between computed and available experimental ^{1}H and ^{13}C chemical shifts is found, providing a firm basis for the above conclusions. Remarkably, the "diamagnetic" corannulene dianion observed in NMR at low temperature is predicted to be a paramagnetic closed-shell species.

1. Introduction

The synthesis of the polycyclic aromatic hydrocarbon dibenzo[*ghi*,*mno*]fluoranthene, more commonly known as corannulene (**1**), was first reported by Barth and Lawton in 1966.[1] The trivial name (from Latin cor, heart; annula, ring) was suggested to connote the relationship to the parent coronene as well as to imply structural and electronic factors considered to be valid at that time.[2] The 17 steps required to synthesize this very interesting PAH precluded any systematic investigation of the physical and chemical properties of corannulene until a simpler synthesis was developed by Scott et al. some 25 years later.[3] The procedure was optimized further by the same group, culminating in an efficient three-step synthesis of corannulene from commercially available materials.[4] Other methods of synthesis have also now been reported.[5–9]

The popularity of corannulene increased dramatically soon after the discovery[10] and synthesis of buckminsterfullerene in large quantities.[11] Because of its bowl-shaped structure, formed by a central pentagonal ring surrounded by five hexagonal rings, corannulene constitutes a multirepeated minimum subunit of all fullerene cages. For that reason, corannulene has become one of the favorite models for studying many of the physical and chemical properties of fullerenes.

Since the very beginning of corannulene history, chemists have been fascinated by the "annulene-within-an-annulene" (AWA) model, in which both rim and hub attain aromatic $4n + 2$ Hückel counts by the transfer of one electron from the rim to the central pentagon.[1] This is also what is expected for two decoupled annulenes with orbital occupancies determined by the aufbau principle: In the Hückel approximation, the two uncoupled annulenes taken together have a doubly degenerate lowest unoccupied molecular orbital (LUMO) totally localized on the rim at 0.209β-α and a pair of doubly degenerate highest occupied molecular orbitals (HOMOs), two localized on the rim and two localized on the hub, at -0.618β-α.

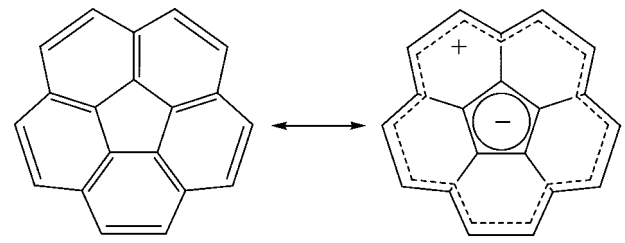

Corannulene Annulene-within-an-annulene (AWA)

Although it was already known that the shortest bonds of corannulene are the radial bonds joining the two concentric rings[2] and that the two rings are therefore strongly coupled, the

* To whom correspondence should be addressed. E-mail: rzanasi@unisa.it.
† Università degli Studi di Salerno.
‡ Boston College.

10.1021/jp8038779 CCC: $40.75
Published on Web 08/12/2008

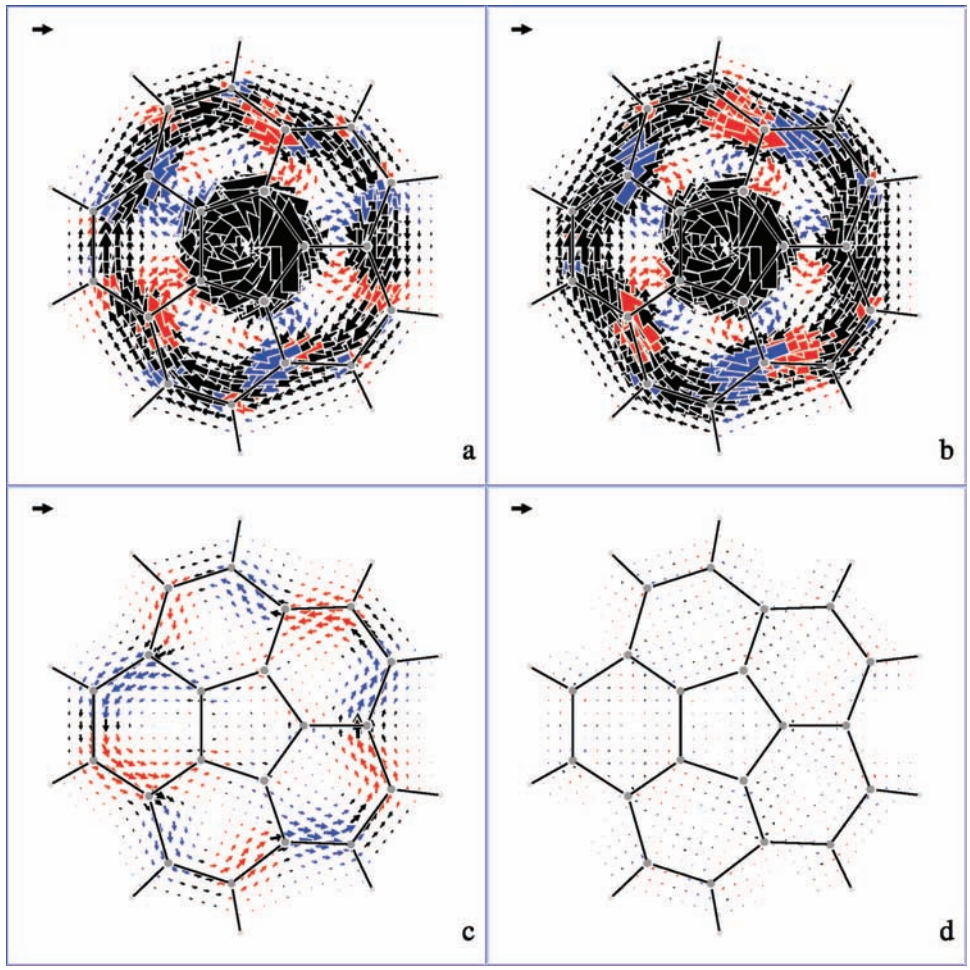

Figure 1. Maps of probability current density induced in the π-system of the C_s-symmetric corannulene dianion ($\mathbf{1}^{2-}$) by a perpendicular external magnetic field pointing toward the viewer. The probability current density is calculated at the ab initio CTOCD-DZ2/6-31G**//B3LYP/6-31G* level and plotted on a surface having the molecular shape at 1 bohr inside the bowl. Keys: (a) total probability current density arising from the set of 11 π-orbitals; (b) two-electron contribution of a″ HOMO; (c) eight-electron contribution from HOMO − 1 to HOMO − 4; and (d) contribution arising from all but the 10 electrons in HOMO, HOMO − 1,..., and HOMO − 4. Arrows indicate the direction and relative magnitude of the probability current density vector. Diatropic/paratropic currents are represented by anticlockwise/clockwise circulations. The black arrow in each upper left corner represents the magnitude of the benzene ring current for its maximum value (j_{max} = 0.080 au) calculated using the same level of theory, to be compared with j_{max} in (a) 0.359, (b) 0.335, (c) 0.072, and (d) 0.020 au. Colors are used to represent the leapfrog character of the circulation: Red (blue) implies that the probability current density vector has a component parallel (antiparallel) to the magnetic field not smaller than the 10% of the vector modulus.

AWA model was considered an attractive hypothesis, and many of the properties of corannulene were justified by adopting such a picture. A number of results reporting calculated populations,[12] nucleus-independent chemical shifts,[13] and current density maps[14] have been presented that point to the inapplicability of the AWA model to corannulene. The most convincing one, in our opinion, shows that corannulene, as well as coronene, sustains counter-rotating ring currents, which are diatropic (aromatic) on the outer rim and paratropic (antiaromatic) on the inner hub,[14] in striking contrast with the AWA model, which predicts con-rotating diatropic ring currents on both rim and hub cycles. It is worthwhile to recall that a paratropic ring current on the five-membered cycles of C_{60} is predicted in both π-only[15] and all-electron[16] calculations and that such a prediction is confirmed by the experimental observation of significant downfield shifts of protons sitting above pentagonal sites in some C_{60} derivatives.[17]

Other very interesting systems characterized by counter-rotating diatropic-rim/paratropic-hub ring currents have been recently reported in the literature, namely, kekulene[18] and [7]circulene.[19] In particular, the strong similarities of the ring current pattern in [*n*]circulenes with $n = 5$ (**1**), 6, and 7 have led to the formulation of a simple model for counter-rotating circulations in [*n*]circulenes.[19] The model describes the ring current patterns of [*n*]circulenes in terms of a coupling strength parameter that charts the variation from the decoupled con-rotating currents of the AWA model to the fully coupled counter-rotating currents of real [*n*]circulenes. Counter-rotating rim and hub currents in coronene have also been rationalized in terms of superposition of all circuit currents, that is, currents induced formally in all possible cyclic paths in the π-system.[20]

In a relatively old paper,[21] reporting calculations in the Hückel approximation, Ege and Vogler anticipated a number of possible ring current patterns for a series of alternant corannulenes, in which both inner and outer perimeters contain $(4n + 2)$ or $(4n)$ carbons. Ege and Vogler reported ring current patterns for decoupled perimeters, that is, AWA systems, as well as for coupled perimeters. Interestingly, for coupled perimeters, Ege and Vogler predicted the same concentric diatropic-rim/paratropic-hub pattern for both $(4n + 2)$- and $(4n)$-corannulenes.[21]

One very simple argument for the AWA model failure in the case of corannulene is the Kekulé count, that is, each of the

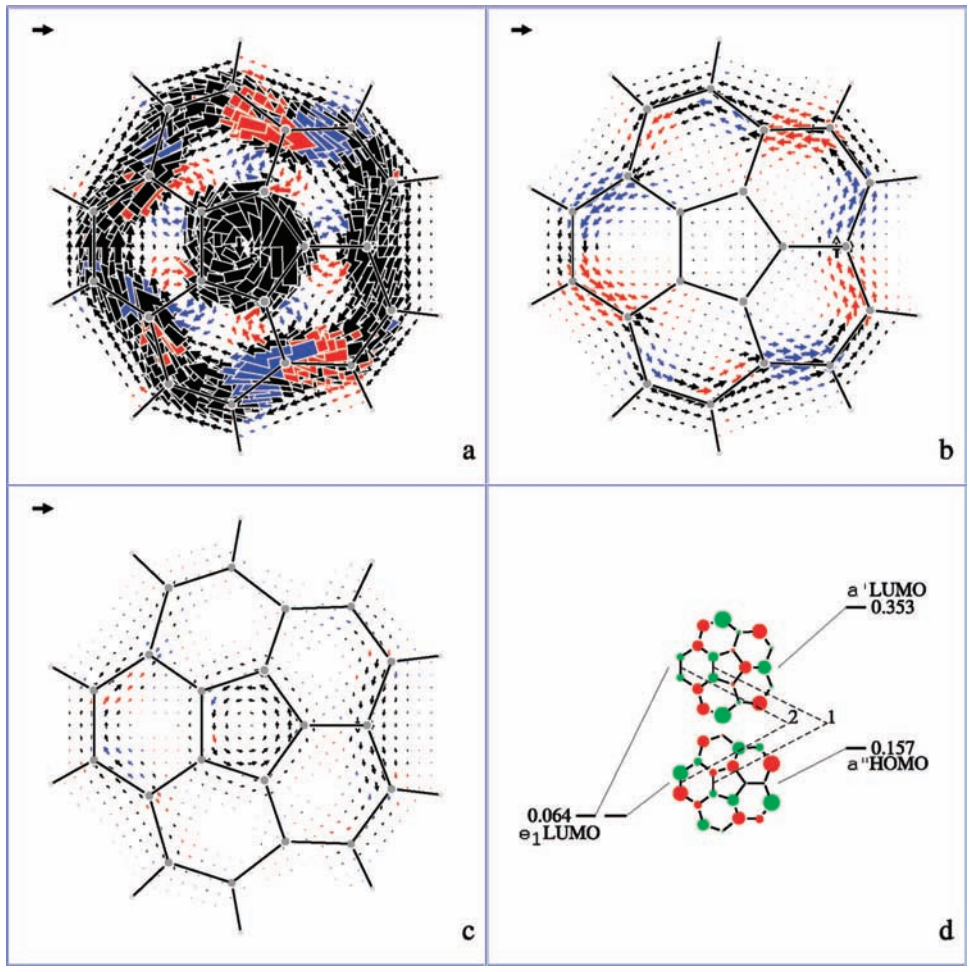

Figure 2. Spectral decomposition of the probability current density arising from the HOMO of $\mathbf{1}^{2-}$. Keys: (a) rotational (and translational) a″ → a′ virtual excitation to the LUMO; (b) the sum of translational a″ → a″ virtual excitation to the LUMO + 1 and translational (and rotational) a″ → a′ virtual excitation to the LUMO + 2; (c) the sum of all but the three lowest energy virtual excitations to LUMO, LUMO + 1, and LUMO + 2. Other details are as in Figure 1. (d) The Jahn−Teller splitting of e_1 LUMO of neutral corannulene into a″ HOMO and a′ LUMO of dianion; ab initio HF orbital energies are in Hartrees, and orbital node structures are from Hückel calculation. Points 1 and 2 indicate regions on inner and outer perimeters where the HOMO presents an inverted orbital combination with respect to the LUMO, thus permitting a prediction of counter-directed currents; see the text for details.

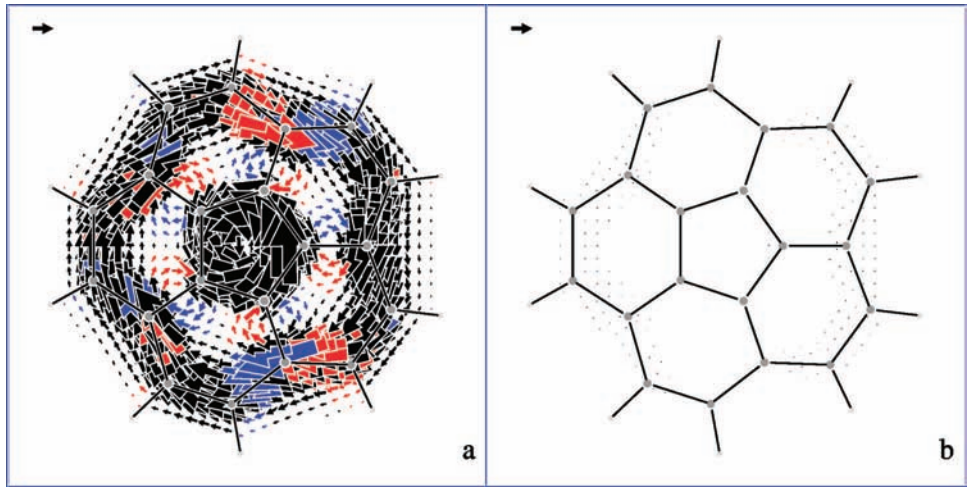

Figure 3. Rotational and translational components of the contribution to the probability current density due to the virtual excitation from a″ HOMO to a′ LUMO of $\mathbf{1}^{2-}$. Keys: (a) rotational component and (b) translational component. Other details are as in Figure 1.

five radial bonds is double in five of the 11 resonance structures. Conversely, a near AWA behavior is expected for coronene-like systems where the radial bonds connecting the two concentric rings are single bonds. It can be shown that such systems can be devised according to the following theorem: Given a system formed by two linked conjugated subsystems of atoms (say carbons), at least one of which is alternant, with separate Kekulé counts designed by K_1 and K_2, respectively, if the alternant subsystem is linked to the other one only by the starred atoms, then the Kekulé count K for the whole system is

TABLE 1: Experimental and Calculated 6-31G//B3LYP/6-31G* Magnetic Properties of Corannulene Dianion[a]**

shift	expt[b]	CTOCD-PZ2	HF/GIAO	B3LYP/GIAO
δ^C (a)	203	155.23	137.84	206.62
δ^C (b)	154	139.79	123.26	158.70
δ^C (c)	120	116.82	98.26	112.45
δ^H (d)	−5.6	0.63	−0.45	−10.53
χ		212	462	7864

[a] Theoretical results have been calculated using the continuous transformation of the origin of the current density method CTOCD-PZ2 (dumped paramagnetic zero), as available within the SYSMO program,[38] and the gauge including atomic orbital (GIAO) approach, as available within GAUSSIAN03.[35] Isotropic chemical shifts with respect to TMS are in ppm. Computed values are averages over (a) inner, (b) nonhydrogenated outer, (c) hydrogenated outer carbon centers, and (d) hydrogen centers. Averaged magnetizability in 10^{-30} J T^{-2}, the conversion factor from a.u. is $a_0^2\ e^2/m_e = 0.78910394 \times 10^{-30}$ J T^{-2}. [b] Experimental data are from ref 32.

$K = K_1 \times K_2$.[22] The two concentric cycles of a coronene-like system composed of fused benzenoid rings do not fulfill the theorem above. Instead, some circulenes (not yet synthesized) formed by fused pentagons fulfill the theorem and are characterized by nearly independent ring currents flowing on inner and outer cycles. These are [10,5]coronene,[23] in which ring currents are counter-rotating paratropic/rim-diatropic/hub, and [8,5] and [12,5]coronene,[24] where ring currents are con-rotating, being paratropic on both cycles. In general, circulenes formed by fused odd-membered rings fulfill the theorem. A further example is isocoronene, which has been found to have a strong diatropic circulation on the perimeter, reinforced by a weak central circulation in the same sense, instead of the paratropic central circulation of coronene.[25]

The simple argument based on Kekulé count factorization can be applied only to a very limited set of polycyclic conjugated hydrocarbons, and for the other cases, one must resort to more general predictive methods. Recently, it has been shown that allowing for the unique properties of the CTOCD-DZ1 (continuous transformation of the origin of the current density-diamagnetic zero) method,[26,27] also referred to as the ipsocentric distribution of the origin, ring currents in conjugated molecules can be rationalized in terms of a few-electron model based on orbital contributions.[28] According to this model, only electrons in π-orbitals near the Fermi level provide an appreciable contribution to the currents through transitions to higher level virtual orbitals. Besides this energy requirement, rooted in the perturbative approach, each contribution has symmetry selection rules and can be identified as translationally allowed (n_1d) for diamagnetic response, rotationally allowed (n_2p) for paramagnetic response, or both ($n_3$dp) for mixed response, where n_1, n_2, and n_3 are the number of electrons in the transitions.[28b] The method has been applied to many systems.[23–25,28b,29,30]

The work described in this paper started from a theoretical investigation of the magnetic properties of corannulene dianion ($\mathbf{1}^{2-}$) and tetraanion ($\mathbf{1}^{4-}$) in terms of induced probability current density and related ^{1}H and ^{13}C magnetic shieldings. These anions were prepared previously,[31] and their optical absorption, electron paramagnetic resonance (EPR), and nuclear magnetic resonance (NMR) spectra were detected.[32] Of particular interest is the existence of a diamagnetic dianion that can be observed in NMR at low temperature ($T < 230$ K). The very high field proton NMR resonance at −5.6 ppm and extremely low field signal of the hub carbons at 204 ppm are consistent with the presence of a large outer paratropic ring current for the dianion. Conversely, the NMR spectra of **1** and $\mathbf{1}^{4-}$ are consistent with an outer diatropic ring current. Thus, on a purely experimental ground, on changing the oxidation state of corannulene from **1** to $\mathbf{1}^{2-}$ and $\mathbf{1}^{4-}$, the external ring current alternates from being diatropic, paratropic, and diatropic again. Compound $\mathbf{1}^{2-}$ is of special interest because it seems to represent an exception if compared with other circulenes with coupled perimeters, which are all characterized by an outer diatropic ring current.[14,18,19,21] Conversely, a paratropic rim circulation is common in the case of loosely coupled circulenes with a rim containing $4n$ carbons.[21,23,24] To further consider this behavior, we also examined the corannulene dication ($\mathbf{1}^{2+}$), which has been obtained in the gas phase,[33] although its magnetic properties have not yet been determined.

As mentioned before, the magnetic response of **1** has already been successfully rationalized in terms of counter-rotating diatropic/rim-paratropic/hub ring currents; see refs 14 and 28b. Within the same references, it was also indicated, without details, that adding four electrons to **1** to produce the tetraanion is sufficient to reverse the hub current to give concentric diamagnetic ring currents.[14,28b] Therefore, our main target here is to analyze the magnetic response of the diamagnetic dianion and dication. In addition, current density maps for the tetraanion will be presented. Given that, the present paper will deal in particular with the following questions. (i) What is the complete ring current pattern of the dianion? (ii) Is it possible to predict the π-electron circulations of the dianion using simple methods, such as the few-electron model based on orbital contributions? (iii) Given the alternating external ring current patterns for **1**, $\mathbf{1}^{2-}$, and $\mathbf{1}^{4-}$, what is the sense of outer and inner ring currents in the diamagnetic dication ($\mathbf{1}^{2+}$), if any?

After a description of molecular geometries and computational details and maps of ab initio probability current density,[34] their analysis in terms of orbital contributions and a discussion of the results will be presented for the dianion and dication in two separate sections, respectively. For the dianion, a comparison of the calculated magnetic properties with the available experimental data (NMR ^{1}H and ^{13}C chemical shifts) will be included. As complementary information, probability current density maps and calculated magnetic properties of the tetraanion will also be reported in a third section.

2. Molecular Geometries and Computational Details

Optimum equilibrium geometries have been obtained at the B3LYP/6-31G* level with the GAUSSIAN 03 program package.[35] As has been recently shown,[36] this level of theory gives for **1** a realistic bowl-shaped structure, providing the best agreement with experimental bond distances and bond angles among a number of popular combinations of methods and basis sets. The C_{5v} bowl-shaped geometry of **1** is given in the Supporting Information.

Geometries for the charged species have been worked out starting from the geometry of **1** and following the indication by Sygula and Rabideau.[12] Both the HOMO and the LUMO of **1** are doubly degenerate, and at this level of theory, they are both of e_1 symmetry. The addition of two electrons for the dianion formation gives rise to four new states within the C_{5v} symmetry group, that is, $^3A_2$, $^1A_1$, and $^1E_2$.[12] The singlet C_{5v} states are less stable than the triplet state, but the degenerate $^1E_2$ state can be distorted into two significantly more stable singlet states of lower symmetry, due to the Jahn−Teller effect. To optimize the structure of these singlet states, the geometry of **1** has been slightly distorted to C_s symmetry according to the two possible ways suggested by the LUMO symmetry. In

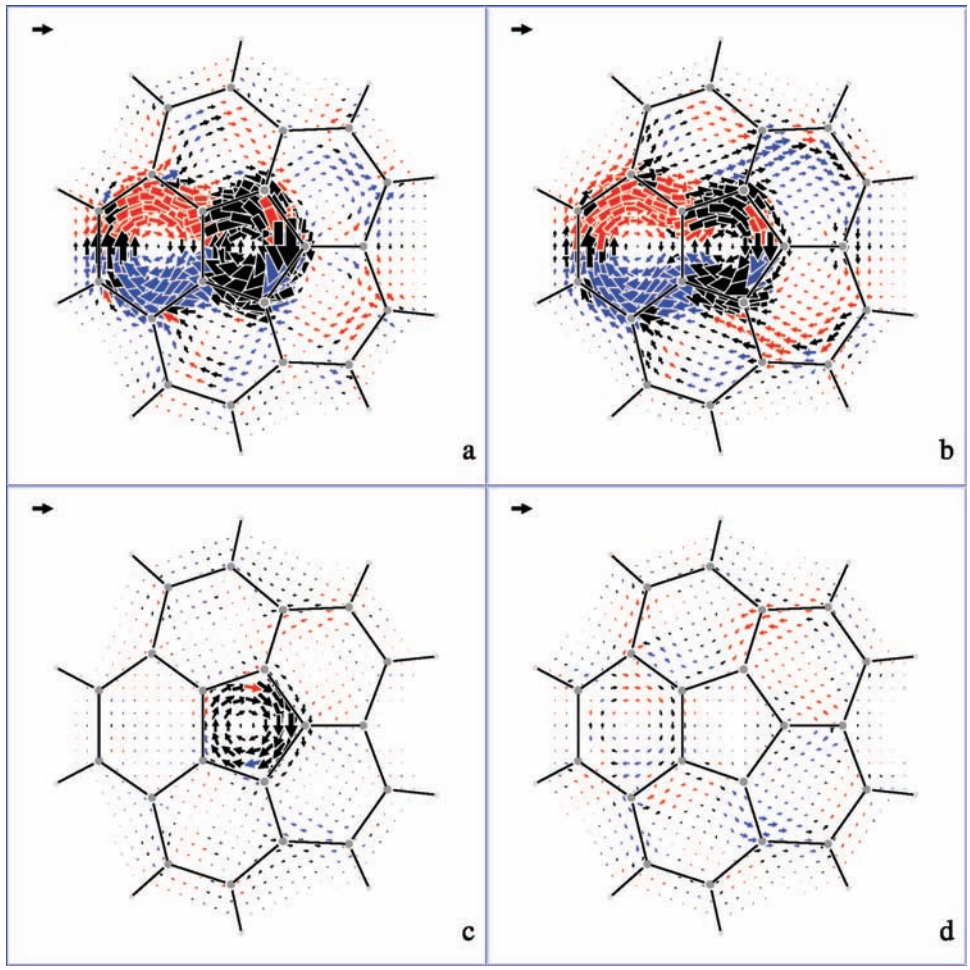

Figure 4. Maps of probability current density induced in the π-system of the C_s-symmetric corannulene dication ($\mathbf{1}^{2+}$). Keys: (a) total probability current density arising from the set of nine π-orbitals; (b) two-electron contributions of a″ HOMO; (c) four-electron contribution from a′ HOMO − 1 and a″ HOMO − 2; and (d) contribution arising from all but the six electrons in HOMO, HOMO − 1, and HOMO − 2. Values of j_{max} are (a) 0.257, (b) 0.194, (c) 0.097, and (d) 0.043 au. Other details are as in Figure 1.

this way, two closed-shell dianions have been identified with a′ and a″ symmetries of their HOMOs, respectively. Hessian calculation has shown that the dianion with HOMO of a″ (a′) symmetry has zero (one) imaginary frequencies, in remarkable agreement with Sygula and Rabideau[12] despite the different method of calculation and basis set. Therefore, the geometry of $\mathbf{1}^{2-}$, for the successive calculation of magnetic properties, has been chosen to be the optimized structure for the singlet with HOMO of a″ symmetry, as the further reduction of symmetry from C_s to C_1 along the vector associated to the imaginary frequency of the singlet with HOMO of a′ symmetry is assumed to provide less important effects on magnetic properties.

The geometry of $\mathbf{1}^{2+}$ has been obtained in much the same way, as the removing of two electrons for the dication formation provides, at this level of theory, an equivalent number and type of states within the C_{5v} symmetry. Distorting the geometry of **1** to the two possible C_s structures, we end up with a closed-shell dication with HOMO of a′ symmetry with zero imaginary frequencies.

For the discussion in the following, it is important to consider the presence of five equivalent bowl-shaped C_s conformations for both $\mathbf{1}^{2-}$ and $\mathbf{1}^{2+}$. These conformations are separated by very low transition energies, which we compute to be as small as 1.0 ($\mathbf{1}^{2-}$) and 1.5 ($\mathbf{1}^{2+}$) kcal mol^{-1}. Because of these small barriers, conformers interconvert quickly, even at low temperature. During the transitions, nuclei undergo only small displacements.

The geometry of $\mathbf{1}^{4-}$ has been readily obtained by adding four electrons for the tetraanion formation and keeping the C_{5v} symmetry. The final structure has no imaginary frequencies, in agreement with Sygula and Rabideau.[12]

The full set of geometries, along with a number of energetic details, is given in the Supporting Information; see Tables S1 and S2 for the dianion, Tables S5 and S6 for the dication, and Tables S9 and S10 for the tetraanion. It should be noticed that the HOMO and HOMO − 1 of $\mathbf{1}^{2+}$ and **1** interchange on passing from the B3LYP/6-31G* to the HF/6-31G** level of theory.

Even for nonplanar molecules, the descendants of π-orbitals of the corresponding planar parents can be easily identified, and they determine the magnetic behavior as found in many systems.[16,24,37] On this ground, we have computed the π-probability current density maps and their decompositions in main orbital contributions presented in the following. The calculations have been carried out at the HF level adopting the CTOCD-DZ2 method,[27] as implemented within the SYSMO package,[38] and the standard 6-31G** basis set. Far from nuclei, CTOCD-DZ1 and CTOCD-DZ2 provide identical results.[27c] Each map shows the calculated probability current density per unit field, induced by an external magnetic field perpendicular to the average plane of carbons forming the central pentagonal ring and pointing toward the viewer, plotted on a surface having

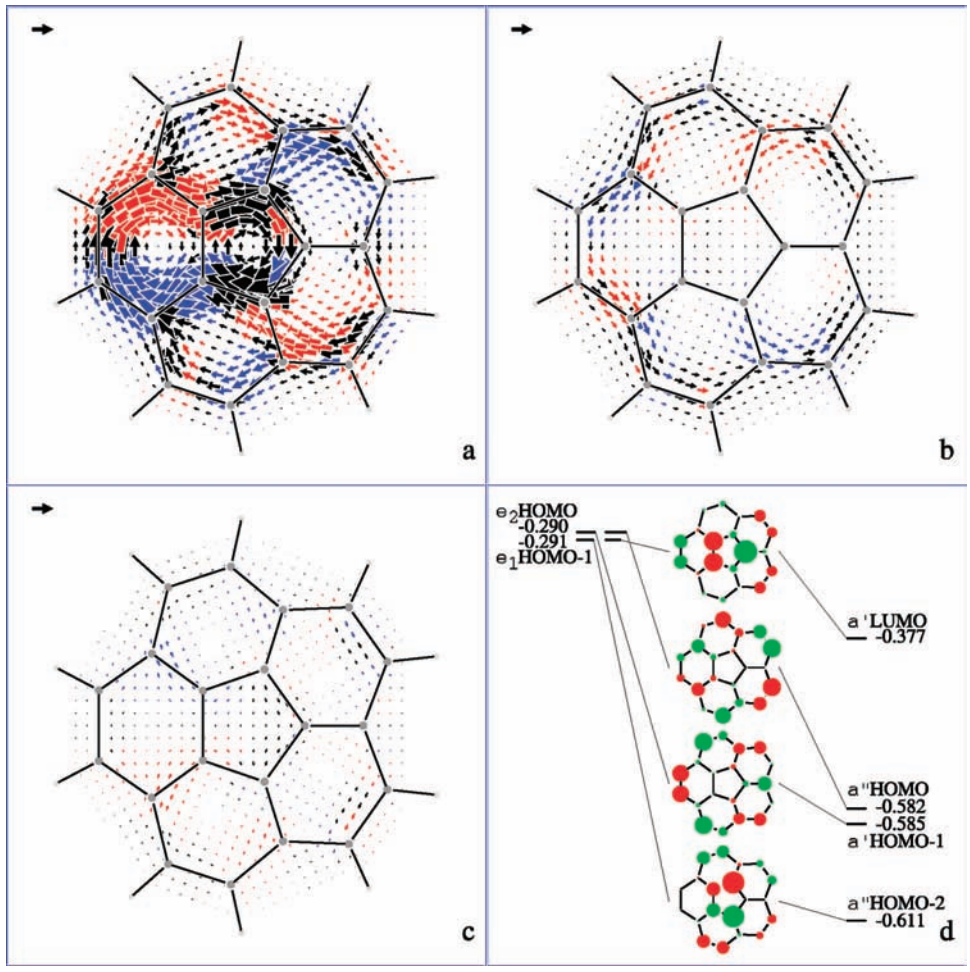

Figure 5. Spectral decomposition of the probability current density arising from the HOMO of $\mathbf{1}^{2+}$. Keys: (a) rotational (and translational) a″ → a′ virtual excitation to the LUMO; (b) the sum of translational a″ → a″ virtual excitation to the LUMO + 1 and translational (and rotational) a″ → a′ virtual excitation to the LUMO + 2; (c) the sum of all but the three lowest energy virtual excitations to LUMO, LUMO + 1, and LUMO + 2. Other details are as in Figure 1. (d) The Jahn−Teller splitting of e_1 HOMO − 1 and e_2 HOMO of neutral corannulene into a″ HOMO − 2, a′ LUMO and a′ HOMO − 1, and a″ HOMO of the dication; ab initio HF orbital energies are in Hartrees, and orbital node structures are from Hückel calculations.

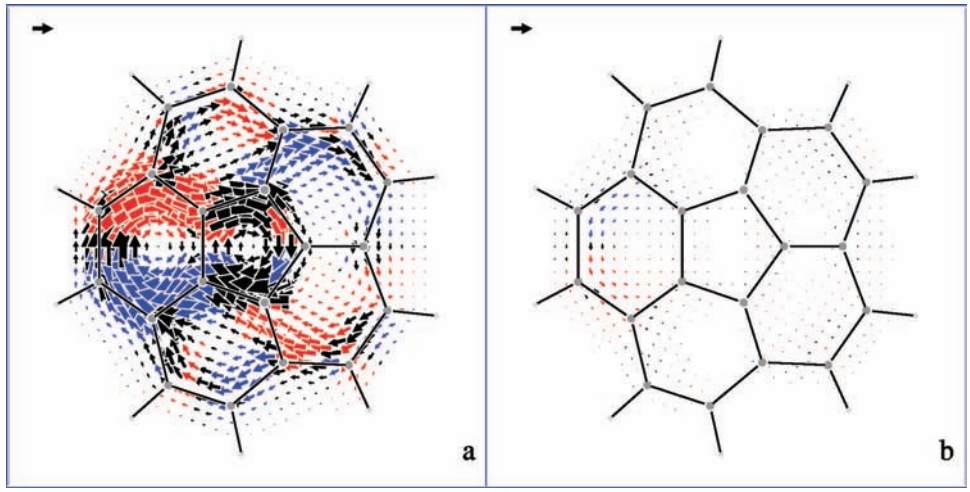

Figure 6. Rotational and translational components of the contribution to the probability current density due to the virtual excitation from a″ HOMO to a′ LUMO of $\mathbf{1}^{2+}$. Keys: (a) rotational component and (b) translational component. Other details are as in Figure 1.

the molecular shape at a distance of 1 bohr from the molecules on the concave side. Arrows indicate the direction and relative magnitude of the probability current density vector. Diatropic currents are represented by anticlockwise circulations, and paratropic currents are represented by clockwise circulations. In all displayed cases, the plotting surface is inside the bowl; on the outside (see Figure S1−S3 of the Supporting Information), currents circulate in much the same way but are weaker, as expected from poorer p-orbitals overlap. Strengths of the different circulations can be judged by the value of j_{max}, the

TABLE 2: Calculated 6-31G//B3LYP/6-31G* Magnetic Properties of Corannulene Dication[a]**

shift	CTOCD-PZ2	HF/GIAO	B3LYP/GIAO
δ^C (a)	154.60	134.33	141.91
δ^C (b)	155.89	136.89	153.10
δ^C (c)	155.66	135.83	145.40
δ^H (d)	7.16	6.45	4.41
χ	−822	−1215	570

[a] See the footnote of Table 1.

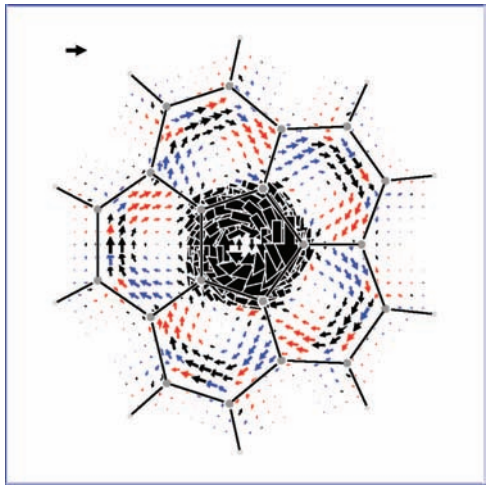

Figure 7. Maps of conformationally averaged probability current density for the π-system of corannulene dication ($\mathbf{1}^{2+}$). The conformational average has been obtained by summing the probability current densities of the five equivalent C_s conformers each weighted by a factor equal to 0.2. Other details are as in Figure 1.

largest modulus of the current density vector per unit inducing field, quoted as a ratio to the corresponding quantity in the 1 bohr plane for benzene, calculated using the same level of theory. This "standard" benzene value is 0.080 au[16] and is represented by the length of the black arrow in the upper left corner of each figure.

Magnetic properties, that is, nuclear magnetic shieldings and magnetizabilities, have been obtained as space integrals of the first-order current density vector field,[27a,b] adopting the dumped paramagnetic-zero (PZ2) variant of the CTOCD method, which is more accurate for this kind of calculation.[27d] Theoretical isotropic chemical shifts have been obtained from computed absolute shieldings according to the following recipes: $\delta^C = 185.60 - \sigma_{Av}(^{13}C) \times 10^6$ for carbon and $\delta^H = 30.80 - \sigma_{Av}(^1H) \times 10^6$ for proton.[27c,d]

3. Corannulene Dianion

Probability current density maps for $\mathbf{1}^{2-}$ (one of the five equivalent C_s conformers) are displayed in Figure 1. As can be observed in panel a, the total probability current density arising from the set of 11 π-orbitals is counter-rotating, being diatropic on the hub and paratropic on the rim, thus providing a first answer to the questions raised at the beginning. One could observe that this pattern of currents is in agreement with the sense predicted by the AWA model (Hückel-based aufbau principle on two uncoupled annulenes), that is, an aromatic 5C/6e hub within an antiaromatic 15C/16e rim,[32] but as it will be shown in a while, the analysis of the orbital contributions does not support this picture and the agreement should be considered as merely fortuitous. According to the j_{max} value, $\mathbf{1}^{2-}$ is characterized by rather strong ring currents. In fact, the total π-current strength is found to be 4.5 times larger than in benzene. Noticeably, the inner diatropic circulation is stronger than the outer paratropic circulation.

Partitioning of the total π-probability current density into its orbital contributions is shown in the other panels of Figure 1: (b) contribution arising from the HOMO; (c) sum of contributions (similar in size) from HOMO − 1 to HOMO − 4; and (d) sum of contributions from all but HOMO, HOMO − 1,..., and HOMO − 4. Remarkably, the HOMO contribution alone gives almost quantitatively the total π-probability current density, despite the diatropic circulation on the outer cycle shown in panel c, whose strength is comparatively much lower. Therefore, the HOMO dominates the magnetic response of $\mathbf{1}^{2-}$, being responsible for both inner (diatropic) and outer (paratropic) strong circulations.

The outer paratropic circulation is consistent with the fact that on Jahn−Teller distortion the degenerate e_1 LUMO of neutral corannulene splits into the a″ HOMO and a′ LUMO of the dianion (see Figure 2d), thus providing a rotationally allowed transition between these two orbitals.[28] Because the HOMO−LUMO gap is small (see Table S2 of the Supporting Information), it is straightforward to predict a rather strong paratropic current for the dianion. Strictly speaking, this transition is also translationally allowed, but the diatropic contribution is expected to be negligible, being the HOMO and the LUMO the descendant of e_1 orbitals.[28] Therefore, less straightforward is to understand the origin of the stronger hub diatropic circulation, since a virtual transition to a higher virtual molecular orbital would account for it, but the bigger gap would contrast with its large strength. The ideal tool to explore this question is the spectral decomposition of ring currents recently introduced by Steiner, Soncini, and Fowler.[39] The breakdown of the HOMO contribution to the probability current density into explicit contributions from virtual excitations is shown in Figure 2a−c. As can be observed, the contribution of the virtual excitation from a″ HOMO to a′ LUMO (panel a), allowed under a rotational (and translational) selection rule, dominates the current, which originates from the HOMO. Relatively small diatropic circulations localized on the rim (panel b, sum of contributions from virtual excitations to LUMO + 1 and LUMO + 2) and on the hub (panel c, sum of contributions from all of the remaining virtual excitations) do not alter the almost perfect overlap of maps in Figures 1b and 2a, which are practically indistinguishable. Therefore, a single virtual excitation from HOMO to LUMO accounts for both the paratropic/rim and the diatropic/hub circulations of $\mathbf{1}^{2-}$, the remaining contributions from each other virtual excitations (and each other occupied orbitals) being comparatively much lower and unimportant. This single HOMO−LUMO contribution to the CTOCD-DZ1 current density deserves a more careful examination. Employing a previously introduced notation,[27] real orbitals and coefficients and sum over repeated Greek indices, such a contribution, $\mathbf{J}^{(1)}_{(H\to L)}$, can be written as a sum of a rotational $\mathbf{J}^{rot}_{(H\to L)}$ and a translational $\mathbf{J}^{tra}_{(H\to L)}$ component:[40]

$$J^{(1)}_{(H\to L)\delta}(\mathbf{r}) = J^{rot}_{(H\to L)\delta}(\mathbf{r}) + J^{tra}_{(H\to L)\delta}(\mathbf{r})$$

$$J^{rot}_{(H\to L)\delta}(\mathbf{r}) = \frac{2e\hbar^2}{m_e} G_\delta(\mathbf{r}) \Gamma^{(\mathbf{r}\times\nabla)_\gamma}_{H,L} B_\gamma \qquad (1)$$

$$J^{tra}_{(H\to L)\delta}(\mathbf{r}) = \frac{2e\hbar^2}{m_e} G_\delta(\mathbf{r}) \varepsilon_{\alpha\beta\gamma} r_\beta \Gamma^{(\nabla)_\alpha}_{H,L} B_\gamma \qquad (2)$$

where

$$G_\delta(\mathbf{r}) = \varphi_H^{(0)}(\mathbf{r})\nabla_\delta\varphi_L^{(0)}(\mathbf{r}) - \varphi_L^{(0)}(\mathbf{r})\nabla_\delta\varphi_H^{(0)}(\mathbf{r})$$

and $\varphi_H^{(0)}$ and $\varphi_L^{(0)}$ are the unperturbed self-consistent field HOMO and LUMO, respectively, $\boldsymbol{\varepsilon}$is the antisymmetric Levi-Civita tensor, $\boldsymbol{\Gamma}_{H,L}^{(\mathbf{r}\times\nabla)}$ and $\boldsymbol{\Gamma}_{H,L}^{(\nabla)}$ are vectors representing rotational and translational selection rules for the HOMO→LUMO transition, respectively, and **B** is the external magnetic field. The rotational and translational components can be mapped separately. For $\mathbf{1}^{2-}$, the calculation gives $\Gamma_{H,L}^{(\mathbf{r}\times\nabla)_\parallel} = 71.4$ and $\Gamma_{H,L}^{(\nabla)_\perp} = -0.2$ au, and as unequivocally shown in Figure 3, only the rotational component (1) is active (panel a), the translational component (2) having practically vanished all over the plotting surface (panel b). In other words, the rotational component alone is responsible not only for the paratropic/rim but also for the diatropic/hub ring current. This singular magnetic response is thus dominated by two electrons through a rotationally allowed transition, leading to the description of corannulene dianion as a (2p) system,[28] with p indicating a paramagnetic response, which, as this case clearly shows, does not imply the absence of diatropic circulations.

To fully understand the origin of the diatropic inner circulation, it is important to consider that according to eq 1, the current pattern is only determined by the spatial distribution of the HOMO and the LUMO, being $\Gamma_{H,L}^{(\mathbf{r}\times\nabla)_\parallel}$ a scale factor whose sign changes according to the sign of $\varphi_H^{(0)}$ and $\varphi_L^{(0)}$. For $\mathbf{1}^{2-}$, these orbitals are nearly uniformly distributed over inner and outer cycles. Let us consider a pair of points $\mathbf{r}_1$ and $\mathbf{r}_2$ facing each other on the two perimeters as in Figure 2d and lying on a nodal surface of the HOMO. In these two points, the expression of the $\mathbf{G}(\mathbf{r})$ field in eq 1 simplifies to $\mathbf{G}(\mathbf{r}_1) = -\varphi_L^{(0)}(\mathbf{r}_1)\nabla\varphi_H^{(0)}(\mathbf{r}_1)$ and $\mathbf{G}(\mathbf{r}_2) = -\varphi_L^{(0)}(\mathbf{r}_2)\nabla\varphi_H^{(0)}(\mathbf{r}_2)$. In these two points, the sign of the LUMO is the same, whereas the gradient of the HOMO reverses as clearly seen in Figure 2d. Therefore, the current in these two points is counter-directed. On close examination, it can be observed that this argument applies to all other facing pairs around the molecule, thus resulting in two counter-rotating circulations. As shown in a more general way elsewhere,[40] the relative tropicity of the ring currents is determined as follows: if the HOMO and the LUMO are both in-phase or out-of-phase combinations of orbitals localized on the two perimeters, then the ring currents are con-rotating, else the ring currents are counter-rotating. For $\mathbf{1}^{2-}$, the HOMO and LUMO are out-of-phase combinations of such localized orbitals.[40a] Hence, assuming an outer paratropic circulation, as required by the stabilization of the molecule in the external magnetic field because of the larger area, the inner circulation is diatropic. Other (2p) circulenes characterized by an inner diatropic ring current have been found. In particular, coronene dianion and dication display this kind of magnetic response.[40b]

The solid foundation of the arguments given above is verified by computing integral properties of the current density, in particular nuclear magnetic shieldings, and comparing the results

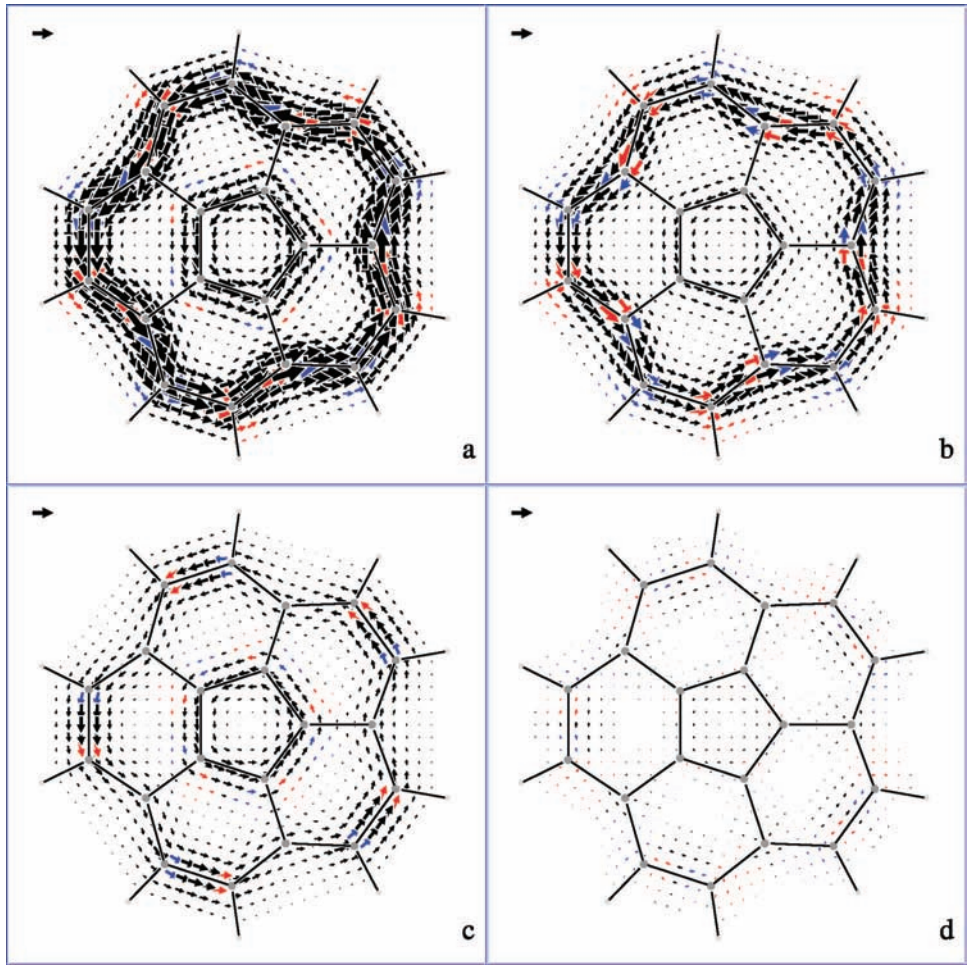

Figure 8. Maps of probability current density induced in the π-system of the C_{5v}-symmetric corannulene tetraanion ($\mathbf{1}^{4-}$). Keys: (a) total probability current density arising from the set of 12 π-orbitals; (b) four-electron contributions of e_1 HOMO pair; (c) four-electron contribution of e_1 HOMO − 1 pair; and (d) contribution arising from all but the eight electrons in HOMO and HOMO − 1 pairs. Values of j_{max} are (a) 0.146, (b) 0.094, (c) 0.061, and (d) 0.020 au. Other details are as in Figure 1.

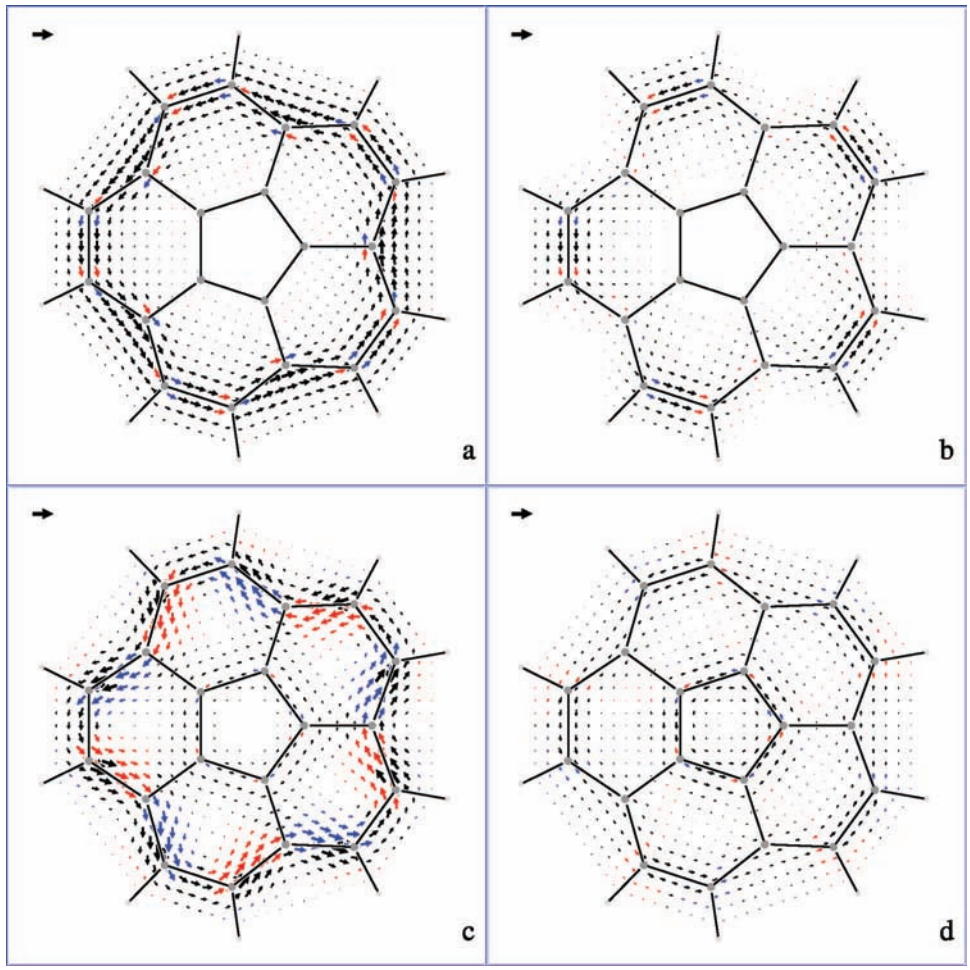

Figure 9. Selection of virtual excitation contributions to the probability current density arising from the e_1 HOMO and e_1 HOMO − 1 of $\mathbf{1}^{4-}$. Keys: (a and b) translational $e_1 \rightarrow a_2$ virtual excitation form HOMO (a) and HOMO − 1 (b) to LUMO; (c) the sum of translational $e_1 \rightarrow a_1$ virtual excitation from HOMO to LUMO + 1 and translational $e_1 \rightarrow e_2$ virtual excitation from HOMO to LUMO + 4; and (d) the sum of translational $e_1 \rightarrow a_1$ virtual excitation from HOMO − 1 to LUMO + 1 and translational $e_1 \rightarrow e_2$ virtual excitation from HOMO − 1 to LUMO + 4. Other details are as in Figure 1.

TABLE 3: Experimental and Calculated 6-31G//B3LYP/6-31G* Magnetic Properties of Corannulene Tetraanion[a]**

shift	expt[b]	CTOCD-PZ2	HF/GIAO	B3LYP/GIAO
δ^C (a)	95.15	91.77	73.71	85.56
δ^C (b)	112.33	116.82	102.34	106.09
δ^C (c)	87.35	89.20	65.06	71.76
δ^C (d)	6.92	6.12	5.20	4.98
χ		−5197	−5669	−5008

[a] See the footnote of Table 1. [b] Experimental data are from ref 32.

with the available experimental data of ^{1}H and ^{13}C NMR chemical shifts. In Table 1, we report theoretically derived isotropic chemical shifts δ's and computed mean magnetizability χ for $\mathbf{1}^{2-}$ together with experimental shifts.[32] (The full set of nuclear magnetic shielding and magnetizability tensor components of $\mathbf{1}^{2-}$ is reported in Tables S3 and S4 of the Supporting Information.) Because of the very small barrier between each of the five degenerate C_s conformations, Table 1 reports averages over (a) inner, (b) nonhydrogenated outer, and (c) hydrogenated outer carbon atoms and (d) hydrogen atoms. This conformational averaging is consistent with the fact that only one NMR signal for each set of atoms is observed for the dianion.[32]

Although the quantitative agreement between CTOCD-PZ2 and experimental isotropic shifts is not particularly good, the NMR signal assignment is safe and consistent with the current patterns shown in Figure 1a. The same is valid also for the HF/GIAO results. For B3LYP/GIAO, the comparison is much better for carbon shifts, whereas protons are predicted to resonate at an exceptionally high field. This result can be understood considering that B3LYP provides a very small (and probably badly underestimated[41]) HOMO−LUMO gap (see Table S2 of the Supporting Information). This is associated with the tendency of many DFT functionals to exaggerate paramagnetism. On the other hand, the HF predictions have the opposite tendency; that is, transition energies are often overestimated, leading to an exaggeration of diamagnetism. Together, these observations provide a picture that is fully consistent with the results reported in Table 1, namely, the experimental proton shift is more or less halfway between HF and B3LYP estimates. Remarkably, according to the magnetizability results of Table 1, the "diamagnetic" dianion observed in NMR at low temperature[32] is predicted to be a paramagnetic closed-shell species.

Thus, considering the lack of significant deviations and the overall satisfactory comparison between theoretical and experimental NMR shifts, we conclude that, although the exact balance of inner and outer currents could be improved, the probability current density patterns shown in Figures 1–3 are correct representations of the response of corannulene dianion to an external magnetic field.

4. Corannulene Dication

Probability current density maps for $\mathbf{1}^{2+}$ (one of the five equivalent C_s conformers) are displayed in Figure 4. The set of 9 π-orbitals (panel a) sustains a single paratropic circulation localized on one indene subunit bisected by the symmetry plane, whose strength is found to be 3.2 times larger than in benzene. The loss of four symmetry planes passing form **1** to $\mathbf{1}^{2+}$ can be expected to lead to more complex current patterns. However, the extent of the deformation is not determined by symmetry, as the qualitatively different patterns of corannulene dianion and dication clearly show. To fully understand the current density pattern, we are prompted to analyze the orbital contributions. Orbital decomposition shows that the HOMO contribution (panel b) dominates the magnetic response of the dication and that a sum of contributions from HOMO − 1 and HOMO − 2 provides a relatively smaller paratropic/hub current (panel c), which reinforces the inner circulation in the total map. The remaining occupied π-orbitals provide a vanishing contribution (panel d). The most significant feature of the magnetic response of $\mathbf{1}^{2+}$ is then a paratropic circulation localized on one indene subunit, which arises from the HOMO.

The removal of two electrons from **1** and the subsequent Jahn−Teller distortion causes a significant rearrangement of the orbital levels. Inspection of the HF orbitals reveals that the degenerate e_1 HOMO − 1 and e_2 HOMO of neutral corannulene evolve, respectively, to a″ HOMO − 2 and a′ LUMO and to a′ HOMO − 1 and a″ HOMO of the dication (see Figure 5d). The splitting of e_1 orbitals into HOMO − 2 and LUMO is consistent with the fact that the Jahn−Teller distorted geometry has two short facing bonds in the hub. No such simple correlation is present for the splitting of e_2 orbitals; indeed, the energy differences of HOMO and HOMO − 1 are very small, and it is even reversed on switching from HF to DFT. The dominant paratropic HOMO contribution is therefore compatible with the rotationally (and translationally) allowed virtual excitation from the a″ HOMO to the a′ LUMO and with the gap, which is as small as those of the dianion (see Table S6 of the Supporting Information).

The breakdown of the HOMO contribution to the probability current density of $\mathbf{1}^{2+}$ into contributions from virtual excitations is shown in Figure 5a−c. Also, in this case, it can be observed that the contribution of the virtual excitation from a″ HOMO to a′ LUMO (panel a), allowed under rotational (and translational) selection rule, dominates the current that originates from the HOMO. A relatively small diatropic/rim circulation (sum of contributions from virtual excitations to LUMO + 1 and LUMO + 2) can be observed in panel b; the sum of contributions from all of the remaining virtual excitations shown in panel c provides an irrelevant circulation. Therefore, a single virtual excitation from HOMO to LUMO accounts for the paratropic circulations localized on one indene subunit of the dication. The further breakdown into rotational (1) and translational (2) components, shown in Figure 6, reveals that the rotational component alone (panel a) provides the main features of the magnetic response of $\mathbf{1}^{2+}$, the translational component (panel b) being vanishingly small. This is also illustrated by the computed values of $\Gamma_{H,L}^{(\mathbf{r}\times\nabla)_\parallel} = 44.5$ and $\Gamma_{H,L}^{(\nabla)_\perp} = 1.1$ au. Using the shorthand introduced in ref 28, corannulene dication is a (2p) system, and according to eq 1, the localization of the circulation on one indene subunit is fully determined by the spatial distribution of the HOMO and the LUMO. Notably, the indene subunit has the same number of radial nodes in both the HOMO and the LUMO, which, considering the behavior of annulenes, would be consistent with localization of the current.

Theoretically derived isotropic chemical shifts δ's and computed mean magnetizability χ for $\mathbf{1}^{2+}$ are collected in Table 2. Also, in this case, because of the very small barrier between conformers, averages over (a) inner, (b) nonhydrogenated outer, and (c) hydrogenated outer carbon atoms and (d) hydrogen atoms are reported. As far as we know, no experimental data are available for the dication for comparison. Different methods of calculation provide slightly varying results but always within expected limits. (The full set of nuclear magnetic shielding and magnetizability tensor components of $\mathbf{1}^{2+}$ is reported in Tables S7 and S8 of the Supporting Information.)

The current density map for $\mathbf{1}^{2+}$ is markedly different from those of the other oxidation states in that it has no rotational symmetry around the perpendicular axis. However, because of the presence of equivalent conformers separated by small energy barriers, measurements in condensed phase either with characteristic times much longer than the time of conformational interconversion (e.g., NMR[42]) or with a sampling volume much larger than molecular volume (e.g., Cotton−Mouton determination of magnetizability) will be sensitive to Boltzmann-averaged properties. As it is possible to track experimentally not only isotropic magnetic responses but also single components of tensor responses,[43] the Boltzmann average can be required also for single components.

The conformational average of a magnetic property can be recast analytically as a magnetic property stemming from a conformationally averaged current density. As long as single components are observed, the conformationally averaged current density has a one-to-one relationship with observables, and thus, it is a well-defined physical quantity, no different than the current density of a single species. Assuming the external magnetic field oriented as in Figure 4a, the other four conformers of $\mathbf{1}^{2+}$ show analogous paratropic circulations localized on each different indene subunit, and the conformational averaged probability current density map of $\mathbf{1}^{2+}$ is as shown in Figure 7. It is interesting to see that the resulting pattern consists of two con-rotating paratropic currents.

5. Corannulene Tetraanion

Probability current density maps for the corannulene tetraanion are given here for the first time in Figure 8. The total probability current density arising from the set of 12 π-orbitals (panel a) is con-rotating being diatropic on both inner and outer cycles, in agreement with the indication provided in refs 14 and 28b. The strength of the outer circulation is found to be 1.8 times larger than in benzene, while the strength of the inner circulation is found to be slightly lower than in benzene. Orbital decomposition shows that both HOMO (panel b) and HOMO − 1 (panel c) contribute to the circulation on both perimeters. According to j_{max} values, the HOMO gives 65% of the external current and almost half of the internal current. The remaining occupied π-orbitals provide a vanishing contribution (panel d).

Figure 9 shows some translationally allowed virtual excitation contributions to the probability current density arising from the e_1 HOMO and e_1 HOMO − 1 of $\mathbf{1}^{4-}$. These have been selected for having the three largest $\Gamma_{i,m}^{(\nabla)_\perp}$ values, corresponding to $\varphi_i^{(0)} \rightarrow \varphi_m^{(0)}$ virtual excitations to a_2 LUMO, a_1 LUMO + 1, and e_2 LUMO + 4 from both HOMO and HOMO − 1. Panels a and b show, respectively, the contribution from HOMO and HOMO − 1 to LUMO; in both cases, no circulation can be observed on the inner cycle, as the LUMO is fully localized on

the rim.[40b] Panels c and d show the sum of contributions for transitions to LUMO + 1 and LUMO + 4 from HOMO and HOMO − 1, respectively; an inner diatropic circulation begins to be visible in both cases. To a first approximation, the total π-current on the outer cycle is given by the sum of contributions displayed in Figure 9. To account for the total π-current in the inner cycle, more transitions are required. In particular, some rotationally allowed virtual excitations, not reported here for the sake of space, provide tiny inner diatropic contributions.

An excellent agreement between CTOCD-PZ2 and experimental isotropic shifts can be observed by inspecting Table 3, confirming the good performance of the method, as previously noticed in the case of neutral corannulene.[14] The agreement is especially remarkable, considering that the tetraanion forms tight ion pairs with the lithium counterions,[31,32] which are not included in the calculations. Worse agreement is obtained with the other two methods of calculation. The much lower mean magnetizability of $\mathbf{1}^{4-}$ with respect to the value calculated for **1** (1.75 times lower, according to CTOCD-PZ2 results), which can be almost completely ascribed to the tensor component parallel to the field (see the Supporting Information), is in full agreement with the sense and strength of the calculated currents shown in Figure 8a. (The full set of nuclear magnetic shielding and magnetizability tensor components of $\mathbf{1}^{4-}$ is reported in Table S11 of the Supporting Information.)

6. Conclusion

The results discussed in this paper enable us to answer the opening questions. (i) The magnetic response of corannulene dianion is characterized by strong counter-rotating paratropic/rim-diatropic/hub ring currents arising almost exclusively from the HOMO and where the inner diatropic circulation is stronger than the outer paratropic circulation. Such a result is confirmed by the agreement between experimental and theoretical NMR shifts. (ii) The breakdown in virtual excitation contributions unequivocally shows that the dianion is a (2p) system, in which only the rotationally allowed HOMO−LUMO transition is responsible for both the outer paratropic and the inner diatropic circulations. This is not fully predictable by the few electron model based on orbital contributions originally developed for annulenes,[28] which would account for the inner diatropic circulation by invocating negligible transitions from the a″ HOMO to higher energy empty a″ orbitals. For corannulene dianion, as well as coronene dianion and dication, one must also consider whether the HOMO and LUMO, generated by Jahn−Teller distortion of a degenerate pair, are in-phase or out-of-phase combinations of orbitals localized on inner and outer perimeters.[40] For the three cited cases, these combinations turn out to be out-of-phase, leading to opposite tropicity of inner and outer ring currents. Then, assuming an outer paratropic circulation, as required by the major stability of the molecule in the external magnetic field, the inner circulation is forced to be diatropic. (iii) Corannulene dication is a (2p) system characterized by a paratropic circulation localized on one indene subunit, arising from one single HOMO−LUMO transition. However, averaging over the five equivalent conformers, which are separated only by a very low energy barrier, the current pattern consists of two con-rotating paratropic circulations delocalized on inner and outer cycles.

The analysis of the magnetic response of corannulene tetraanion confirms the presence of con-rotating diatropic ring currents as already indicated in the literature.[14,28b] These currents arise mainly from HOMO and HOMO − 1, which contribute to both inner and outer circulations. In particular, the outer circulation is nearly given by virtual excitations from HOMO and HOMO − 1 to LUMO, LUMO + 1, and LUMO + 4; these same transitions provide only part of the inner circulation, which is completed by several other translationally, as well as rotationally, allowed transitions. A good agreement between computed and experimental isotropic chemical shifts is found.

According to the results obtained here, the three corannulene ions plus the neutral species form a very special set, which spans all of the possible patterns of rim/hub circulations: diatropic/hub-paratropic/rim ($\mathbf{1}^{2-}$), paratropic/hub-paratropic/rim ($\mathbf{1}^{2+}$, when the conformationally averaged current is considered), diatropic/hub-diatropic/rim ($\mathbf{1}^{4-}$), and paratropic/hub-diatropic/rim (**1** as previously reported). This full set of possible patterns of rim and hub circulations for a single molecular topology is here reported for the first time. We are fascinated by the image of the tangential bonds of corannulene as magnetic Euripi, whereby the variation of the occupation numbers of the molecular orbitals acts as the change of pressure that reverses the strong tidal current in the Greek Euripus strait.

Acknowledgment. Financial support from the Italian MURST and the U.S. National Science Foundation is gratefully acknowledged.

Supporting Information Available: Tables of nuclear coordinates, total and orbital energies, and absolute nuclear magnetic shielding constants and maps of probability current density on the convex side of the bowls and for the neutral corannulene. This material is available free of charge via the Internet at http://pubs.acs.org.

References and Notes

(1) Barth, W. E.; Lawton, R. G. *J. Am. Chem. Soc.* **1966**, *88*, 380–381.
(2) Barth, W. E.; Lawton, R. G. *J. Am. Chem. Soc.* **1971**, *93*, 1730–1745.
(3) Scott, L. T.; Hashemi, M. M.; Meyer, D. T.; Warren, H. B. *J. Am. Chem. Soc.* **1991**, *113*, 7082–7084.
(4) Scott, L. T.; Cheng, P.-C.; Hashemi, M. M.; Bratcher, M. S.; Meyer, D. T.; Warren, H. B. *J. Am. Chem. Soc.* **1997**, *119*, 10963–10968.
(5) Borchardt, A.; Fuchicello, A.; Kilway, K. V.; Baldridge, K. K.; Siegel, J. S. *J. Am. Chem. Soc.* **1992**, *114*, 1921–1923.
(6) Zimmermann, G.; Nuechter, U.; Hagen, S.; Nuechter, M. *Tetrahedron Lett.* **1994**, *35*, 4747–4750.
(7) Liu, C. Z.; Rabideau, P. W. *Tetrahedron Lett.* **1996**, *37*, 3437–3440.
(8) Mehta, G.; Panda, G. *Tetrahedron Lett.* **1997**, *38*, 2145–2158.
(9) Seiders, T. J.; Baldridge, K. K.; Siegel, J. S. *J. Am. Chem. Soc.* **1996**, *118*, 2754–2755.
(10) Kroto, H. W.; Heath, J. R.; O'Brien, S. C.; Curl, R. F.; Smalley, R. E. *Nature* **1985**, *318*, 162–163.
(11) Krätschmer, W.; Lamb, L. D.; Fostiropoulos, K.; Huffman, D. R. *Nature* **1990**, *347*, 354–358.
(12) Sygula, A.; Rabideau, P. W. *J. Mol. Struct. THEOCHEM* **1995**, *333*, 215–226.
(13) Bühl, M. *Chem. Eur. J.* **1998**, *4*, 734–739.
(14) Steiner, E.; Fowler, P. W.; Jenneskens, L. W. *Angew. Chem., Int. Ed.* **2001**, *40*, 362–366.
(15) Pasquarello, A.; Schlüter, M.; Haddon, R. C. *Science* **1992**, *257*, 1660–1661.
(16) Zanasi, R.; Fowler, P. W. *Chem. Phys. Lett.* **1995**, *238*, 270–280.
(17) Prato, M.; Suzuki, T.; Wudl, F. *J. Am. Chem. Soc.* **1993**, *115*, 7876–7877.
(18) Steiner, E.; Fowler, P. W.; Jenneskens, L. W.; Acocella, A. *Chem. Commun.* **2001**, 659–660.
(19) Acocella, A.; Havenith, R. W. A.; Steiner, E.; Fowler, P. W.; Jenneskens, L. W. *Chem. Phys. Lett.* **2002**, *363*, 64–72.
(20) Aihara, J. *Chem. Phys. Lett.* **2004**, *393*, 7–11.
(21) Ege, G.; Vogler, H. *Theoret. Chim. Acta* **1972**, *26*, 55–65.
(22) The proof of the theorem is from Kasteleyn's theorem and is given in Monaco, G.; Zanasi, R. Manuscript in preparation.
(23) Monaco, G.; Viglione, R. G.; Zanasi, R.; Fowler, P. W. *J. Phys. Chem. A* **2006**, *110*, 7447–7452.

(24) Monaco, G.; Fowler, P. W.; Lillington, M.; Zanasi, R. *Angew. Chem., Int. Ed.* **2007**, *46*, 1889–1892.

(25) Ciesielski, A.; Cyrański, M. K.; Krygowski, T. M.; Fowler, P. W.; Lillington, M. *J. Org. Chem.* **2006**, *71*, 6840–6845.

(26) Keith, T. A.; Bader, R. F. W. *Chem. Phys. Lett.* **1993**, *210*, 223–231.

(27) (a) Lazzeretti, P.; Malagoli, M.; Zanasi, R. *Chem. Phys. Lett.* **1994**, *220*, 299–304. (b) Coriani, S.; Lazzeretti, P.; Malagoli, M.; Zanasi, R. *Theor. Chim. Acta* **1994**, *89*, 181–192. (c) Zanasi, R.; Lazzeretti, P.; Malagoli, M.; Piccinini, F. *J. Chem. Phys.* **1995**, *102*, 7150–7157. (d) Zanasi, R. *J. Chem. Phys.* **1996**, *105*, 1460–1469.

(28) (a) Steiner, E.; Fowler, P. W. *Chem. Commun.* **2001**, 2220–2221. (b) Steiner, E.; Fowler, P. W. *J. Phys. Chem. A* **2001**, *105*, 9553–9562.

(29) Steiner, E.; Fowler, P. W. *Chem. Phys. Chem.* **2002**, *3*, 114–116.

(30) Cyrański, M. K.; Havenith, R. W. A.; Dobrowolski, M. A.; Gray, B. R.; Krygowski, T. M.; Fowler, P. W.; Jenneskens, L. W. *Chem. Eur. J.* **2007**, *13*, 2201–2207.

(31) (a) Ayalon, A.; Rabinovitz, M.; Cheng, P.-C.; Scott, L. T. *Angew. Chem., Int. Ed. Engl.* **1992**, *31*, 1636–1637. (b) Ayalon, A.; Sygula, A.; Cheng, P.-C.; Rabinovitz, M.; Rabideau, P. W.; Scott, L. T. *Science* **1994**, *265*, 1065–1067. (c) Benshafrut, R.; Shabtai, E.; Rabinovitz, M.; Scott, L. T. *Eur. J. Org. Chem.* **2000**, 1091−1106 and references therein.

(32) Baumgarten, M.; Gherghel, L.; Wagner, M.; Weltz, A.; Rabinovitz, M.; Cheng, P.-C.; Scott, L. T. *J. Am. Chem. Soc.* **1995**, *117*, 6245–6257.

(33) Schröder, D.; Loos, J.; Schwarz, H.; Thissen, R.; Preda, D. V.; Scott, L. T.; Caraiman, D.; Frach, M. V.; Böhme, D. K. *Helv. Chim. Acta* **2001**, *84*, 1625–1634.

(34) For a definition, see Lazzeretti, P. In *Handbook of Molecular Physics and Quantum Chemistry*; Wilson, S., Ed.; John Wiley & Sons, Ltd.: Chichester, 2003; Vol. 3: Molecules in the Physico-Chemical Environment: Spectroscopy, Dinamics and Bulk Properties, Part 1, Chapter 3, pp 53−145.

(35) Frisch, M. J.; Trucks, G. W.; Schlegel, H. B.; Scuseria, G. E.; Robb, M. A.; Cheeseman, J. R.; Montgomery, J. A., Jr.; Vreven, T.; Kudin, K. N.; Burant, J. C.; Millam, J. M.; Iyengar, S. S.; Tomasi, J.; Barone, V.; Mennucci, B.; Cossi, M.; Scalmani, G.; Rega, N.; Petersson, G. A.; Nakatsuji, H.; Hada, M.; Ehara, M.; Toyota, K.; Fukuda, R.; Hasegawa, J.; Ishida, M.; Nakajima, T.; Honda, Y.; Kitao, O.; Nakai, H.; Klene, M.; Li, X.; Knox, J. E.; Hratchian, H. P.; Cross, J. B.; Bakken, V.; Adamo, C.; Jaramillo, J.; Gomperts, R.; Stratmann, R. E.; Yazyev, O.; Austin, A. J.; Cammi, R.; Pomelli, C.; Ochterski, J. W.; Ayala, P. Y.; Morokuma, K.; Voth, G. A.; Salvador, P.; Dannenberg, J. J.; Zakrzewski, V. G.; Dapprich, S.; Daniels, A. D.; Strain, M. C.; Farkas, O.; Malick, D. K.; Rabuck, A. D.; Raghavachari, K.; Foresman, J. B.; Ortiz, J. V.; Cui, Q.; Baboul, A. G.; Clifford, S.; Cioslowski, J.; Stefanov, B. B.; Liu, G.; Liashenko, A.; Piskorz, P.; Komaromi, I.; Martin, R. L.; Fox, D. J.; Keith, T.; Al-Laham, M. A.; Peng, C. Y.; Nanayakkara, A.; Challacombe, M.; Gill, P. M. W.; Johnson, B.; Chen, W.; Wong, M. W.; Gonzalez, C. ; Pople, J. A.; Gaussian 03, Revision B.05; Gaussian, Inc.: Pittsburgh, PA, 2003.

(36) Petrukhina, M. A.; Andreini, K. W.; Mack, J.; Scott, L. T. *J. Org. Chem.* **2005**, *70*, 5713–5716.

(37) Cadioli, B.; Fowler, P. W.; Steiner, E.; Zanasi, R. *J. Phys. Chem. A* **1998**, *102*, 7297–7302.

(38) Lazzeretti, P.; Malagoli, M.; Zanasi, R. SYSMO Package, Universities of Modena and Salerno.

(39) Steiner, E.; Soncini, A.; Fowler, P. W. *J. Chem. Phys. A* **2006**, *110*, 12882–12886.

(40) (a) Monaco, G.; Zanasi, R. AIP Conference Proceedings, **2007**, *963*, 1302−1305. (b) Monaco, G.; Zanasi, R. Int. J. Quantum Chem. In press.

(41) Allen, M. J.; Keal, T. W.; Tozer, D. J. *Chem. Phys. Lett.* **2003**, *380*, 70–77, and references therein.

(42) Jackman, L. M., Cotton, F. A., Eds. *Dynamic Nuclear Magnetic Resonance Spectroscopy*; Academic Press: New York, NY, 1975.

(43) Kumar, A.; Grace, R. C. R.; Madhu, P. K. *Prog. Nucl. Magn. Reson.* **2000**, *37*, 191–319.

JP8038779